

We are IntechOpen, the world's leading publisher of Open Access books Built by scientists, for scientists

6,900

Open access books available

186,000

International authors and editors

200M

Downloads

Our authors are among the

154

Countries delivered to

TOP 1%

most cited scientists

12.2%

Contributors from top 500 universities



WEB OF SCIENCE™

Selection of our books indexed in the Book Citation Index
in Web of Science™ Core Collection (BKCI)

Interested in publishing with us?
Contact book.department@intechopen.com

Numbers displayed above are based on latest data collected.
For more information visit www.intechopen.com



***In Silico* Study of Hydroxyapatite and Bioglass®: How Computational Science Sheds Light on Biomaterials**

Marta Corno, Fabio Chiatti, Alfonso Pedone and Piero Ugliengo
Dipartimento di Chimica I.F.M. and NIS, Università di Torino, Torino
Dipartimento di Chimica, Università di Modena & Reggio Emilia, Modena
Italy

1. Introduction

Hydroxyapatite and Bioglass® are two well-known biomaterials, belonging to the vast class of ceramic supplies, both highly biocompatible and widely applied in the biomedical field. In spite of a huge research regarding engineering applications of both inorganic materials, still many aspects of their tissue integration mechanism have not been completely cleared at a molecular level. Thus, *in silico* studies play a fundamental role in the prediction and analysis of the main interactions occurring at the surface of these biomaterials in contact with the biological fluid when incorporated in the living tissue (prevalently bones or teeth). Hydroxyapatite [HA, $\text{Ca}_{10}(\text{PO}_4)_6(\text{OH})_2$] owes its relevance and use as a biomaterial since it constitutes the majority of the mineral phase of bones and tooth enamel in mammals (Young & Brown, 1982). For sake of completeness, we mention that hydroxyapatite is also studied as an environmental adsorbent of metals and a catalyst (Matsumura & Moffat, 1996; Toulhat et al., 1996). One of the first applications of HA in biomedicine dates back to 1969, when Levitt *et al.* hot-pressed it in powders for biological experimentations (Levitt et al., 1969). From then on, several commercial forms of HA have appeared on the market. The material has also been utilized for preparing apatitic bioceramic, due to its bioresorbability which can be modulated changing the degree of cristallinity. There are so many examples of applications, from Mg^{2+} -substituted hydroxyapatite (Roveri & Palazzo, 2006) to the synthesis of porous hydroxyapatite materials by colloidal processing (Tadic et al., 2004), starch consolidation (Rodriguez-Lorenzo et al., 2002), gel casting (Padilla et al., 2002) and more. Furthermore, recent applications follow a biologically inspired criterion to combine HA to a collagen matrix aiming at the improvement of mechanical properties and bioactivity (Wahl et al., 2007). However, a complete review of all the practical as well as hypothetical uses of HA in the biomaterial area is outside the scope of this Chapter. Inside the bone, a highly hierarchical collagen-mineral composite, hydroxyapatite is in the form of nano-sized mineral platelets (Currey, 1998; Fratzl et al., 2004; Weiner & Wagner, 1998) and contains carbonate ions for the 4-8 weight % (Roveri & Palazzo, 2006). In section 2.1 of this Chapter, two aspects of defects which can be encountered in a synthetic or natural HA sample will be presented. The first aspect deals with non-stoichiometric surfaces and

their adsorptive behavior towards simple molecules (water and carbon monoxide). The second concerns the inclusion of carbonate ions in the pure HA bulk structure to simulate the apatite bone tissue. These examples of applying sophisticated computational techniques to the investigation of defects in HA represent a very recent progress achieved in our laboratory inside this biomedical research area, which has been carried out since 2003. For the interested reader, a summary of the last years work on simulation of HA in our research group has been recently published (Corno et al., 2010).

As for bioactive glasses, the first synthesis was performed in 1969-71 by Larry Hench in Florida (Hench et al., 1971). He had synthesised a silicate-based material containing calcium and phosphate and had implanted this composition in rats' femurs (Hench, 2006). The result was a complete integration of the inorganic material with the damaged bone. This very first composition was called Bioglass® 45S5 (45SiO₂ - 24.5Na₂O - 24.5CaO - 6P₂O₅ in wt. % or 46.1 SiO₂, 24.4 Na₂O, 26.9 CaO and 2.6 P₂O₅ in mol %) and has been introduced in clinical use since 1985. The interest has been then to investigate the steps of the bioactivity mechanism leading to the formation of a strong bond between the material and the biological tissue. The most renowned hypothesis is the so-called Hench mechanism and its crucial step resides in the growth of a thin amorphous layer of hydroxy-carbonated apatite (HCA) (Hench, 1998; Hench & Andersson, 1993; Hench et al., 1971). Indeed, on that layer biological growth factors are adsorbed and desorbed to promote the process of stem cells differentiation. Moreover, before the growth of HCA, several other chemical reactions occur, dealing particularly with the exchange of sodium and calcium ions present in the Bioglass® with protons derived from the biological fluid. The influence of the chemical components of the inorganic material on its bioactivity has recently been object of scientific research and discussion. For instance, additives such as fluorine (Christie et al., 2011; Lusvardi et al., 2008a), boron, magnesium (A. Pedone et al., 2008) and zinc (Aina et al., 2011) were considered in a number of systematic studies. In section 2.2 of this Chapter, the role of phosphate concentration inside models with the 45S5 composition will be highlighted, since these changes in content can affect the crucial mechanism of gene activation and modify the local environment of the silicon framework and of Na and Ca sites, as well as the dissolution rate of silica (O'Donnell et al., 2009).

The joint use of experimental and theoretical techniques nowadays has reached a very large diffusion due to the completeness of the derived information. Particularly, in the biological or biochemical field, computational methods are essential to the investigation of interfacial mechanisms at a molecular level. Moreover, very often the interplay between experimental and calculated data allows researchers to improve both methodologies. A huge amount of examples could be reported, but for sake of brevity here we limit to our own experience of collaboration with a number of experimentalists. Indeed, in our research papers, dealing either with HA or with bioactive glasses, there is always a detailed comparison with measured data, for instance by means of NMR (Pedone et al., 2010), IR and Raman spectroscopy and of adsorption microcalorimetry (Corno et al., 2009; Corno et al., 2008). In our computational studies, we refer to quantum-mechanical techniques, which are very accurate but also quite heavy as for the need of resources. Usually, high parallel computing systems are required to run the simulations and we have successfully used the supercomputers of several HPC centers, such as the Barcelona Supercomputing Centre (Spain) or the CINECA Supercomputing Center (Italy).

The most used theoretical framework in the last decade's literature is the Density Functional Theory, which grants a good compromise in terms of accuracy of the representation and

computational time. Our calculations are performed either with the pure GGA PBE functional (Perdew et al., 1996) or with the hybrid B3LYP (Becke, 1993), both well-known functionals. Two *ab initio* approaches are possible within DFT and they differ for the type of basis set functions. Indeed, a localized Gaussian basis set can be considered, as in the present case, or a plane waves one, also extremely diffuse. An *excursus* of advantages and disadvantages of these approaches is not useful in this context and will be omitted, by focusing exclusively on Gaussian type functions.

2. Hydroxyapatite and Bioglass® as computational case study

All the calculations mentioned in this Chapter have been performed using the CRYSTAL code in its latest release (Dovesi et al., 2005a; Dovesi et al., 2005b; Dovesi et al., 2009). This periodic quantum-mechanical software has been developed by the Theoretical Chemistry group of the University of Turin (Italy) together with the Daresbury Laboratory (UK) since 1988. CRYSTAL is capable of computing systems with every dimensionality, from molecules to real infinite crystals and it supports massive parallel calculations. This code uses local Gaussian basis sets and can deal with many electronic structure methods, from Hartree-Fock to Kohn-Sham Hamiltonians. Structural, electrostatic and vibrational properties of the studied materials have been characterized with the program. Another crucial aspect in modeling is the graphical visualization and representation of structures. For all the images displayed in this Chapter, MOLDRAW (Ugliengo et al., 1993), J-ICE (Canepa et al., 2011b) and VMD (Humphrey et al., 1996) programs were used. Further more precise computational details can be read in a number of our recent papers on both HA (Corno et al., 2009; Corno et al., 2006; Corno et al., 2007; Corno et al., 2010) and bioactive glasses (Corno & Pedone, 2009; Corno et al., 2008).

2.1 Defects in hydroxyapatite bulk and surfaces

Hydroxyapatite (HA) is a mineral which occurs in nature in two polymorphs, a monoclinic form, thermodynamically stable at low temperatures, and an hexagonal form, which can be easily stabilized by substitution of the OH⁻ ions (Suda et al., 1995). These ions are aligned along the *c* axis (the [001] direction), as highlighted in Fig. 1. The single crystal structure of the hexagonal form of HA is characterized by the $P6_3/m$ space group. The mirror plane, perpendicular to the [001] direction, is compatible with the column of OH⁻ ions because of an intrinsic static disorder of these ions, which can point, with no preference, in one of the two opposite directions ([001] or [00-1]). The result is a fractional occupation of the sites in the solved crystallographic structure (50% probability for each direction). As *ab initio* simulation cannot take into account the structural disorder, we reduced the symmetry to $P6_3$, removing the mirror plane and fixing the directions of the OH⁻ ions. In the most stable configuration found, both the OH⁻ ions point in the same direction, as reported in Fig. 1. The oxygen atom of the OH⁻ ion is close to three Ca ions, which form an equilateral triangle in the *ab* plane. Moreover, there are six phosphate ions inside the crystallographic cell, all symmetry equivalent.

The bulk structure of crystalline HA, fully characterized in the literature (Corno et al., 2006), has been considered as a starting point to model the surfaces which are experimentally found to be the most important: (001) in terms of reactivity, and (010) in terms of exposure in the crystal habit (Wierzbicki & Cheung, 2000). Those surfaces have already been fully characterized at an *ab initio* level, and all the structural, geometrical and electronic properties

have been predicted and compared with the experimental values (Corno et al., 2007). More recently, these modeled surfaces were also employed to study the adsorption of different typologies of molecules that span from water (Corno et al., 2009) to organic acids (Canepa et al., 2011a), amino-acids (Rimola et al., 2008) and small peptides (Corno et al., 2010; Rimola et al., 2009), providing results comparable with the experimental heats of adsorption, when available.

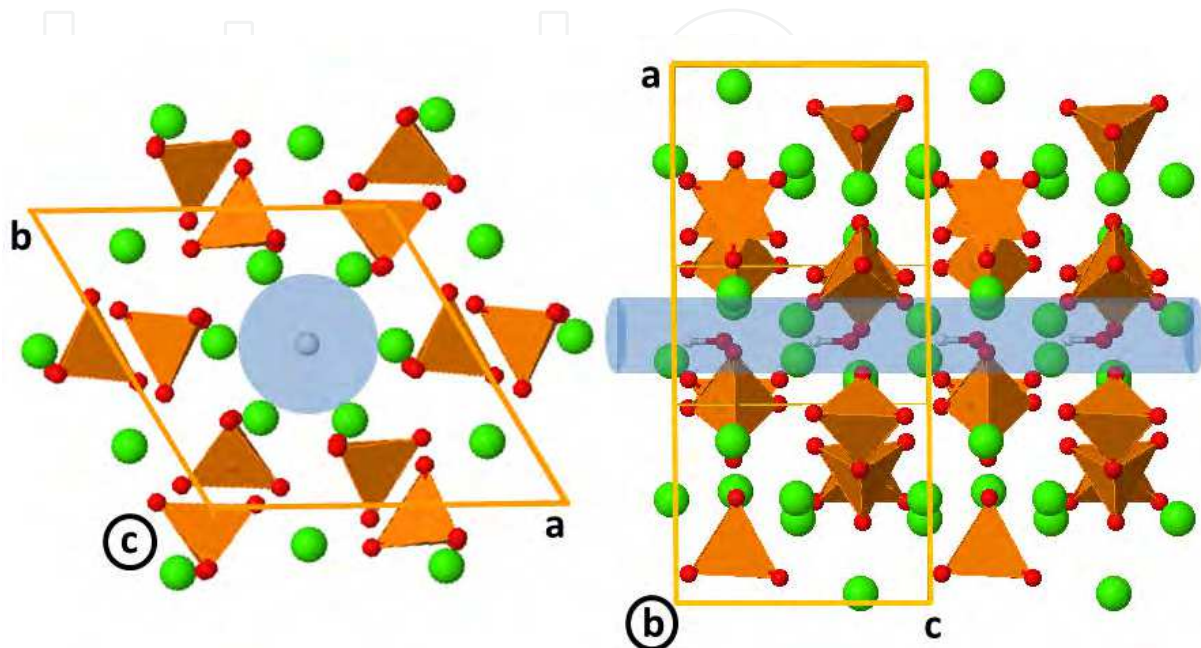


Fig. 1. Two views of the unit cell of the HA bulk structure: calcium in light green, oxygen red, hydrogen light grey and phosphate ions as orange tetrahedra. In the blue cylinders, the column of OH⁻ ions can be observed. Unit cell borders are drawn in light orange.

Nonetheless, the study of the possible terminations along the [010] direction is not yet complete, because two new kinds of (010) surfaces have been discovered experimentally. These surfaces are non-stoichiometric, because their composition is different from the bulk.

2.1.1 The (010) non-stoichiometric surfaces

In 2002, a HRTEM study highlighted three possible terminations for the (010) surface. As a matter of fact, HA shows an alternation of two layers, Ca₃(PO₄)₂ (A-type) and Ca₄(PO₄)₂(OH)₂ (B-type), which can be interrupted in three different ways (Sato et al., 2002). As the sequence is ...-A-A-B-A-A-B-A-A-B..., the periodicity can be truncated by exposing as last layers ...-A-B-A or ...-A-A-B or ...-B-A-A, as shown in Fig. 2. As already done in previous work with other surfaces, we investigated these three possible structures with a slab approach. From the bulk, we extracted a piece of matter along the desired direction, in this case the [010], generating two faces which are exposed to vacuum. These faces ought to be the same to remove any possible dipole moment across the slab, due to geometrical dissimilarities. This necessity may bring the loss of stoichiometricity, in terms of the possibility of obtaining the bulk by replicating the slab along the non-periodic direction: neither B-A-A-B-A-A-B nor A-A-B-A-A-B-A-A can be replicated to regenerate the bulk. Only the stoichiometric surface, characterized by a Ca/P ratio of 1.67, maintains the bulk sequence A-B-A-A-B-A. The slab structure terminating in -A-A-B is called *Ca-rich* (010)

surface as its Ca/P ratio increases to 1.71. The last one is called *P-rich* (010) surface, with a Ca/P ratio of 1.62.

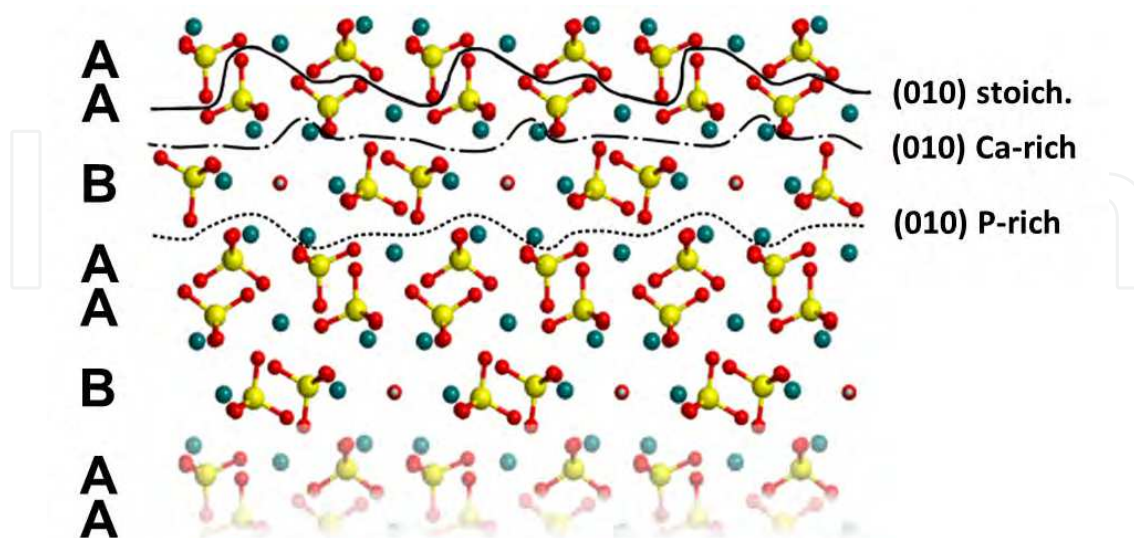


Fig. 2. The three possible terminations along the [010] direction of HA. Colour coding: calcium cyan, oxygen red, hydrogen grey and phosphorous yellow.

Clearly, due to the non-stoichiometric nature of these new surfaces, E_{surf} cannot be defined using the classical formula:

$$E_{\text{surf}} = (E_{\text{slab}} - n \cdot E_{\text{bulk}}) / (2 \cdot A) \quad (1)$$

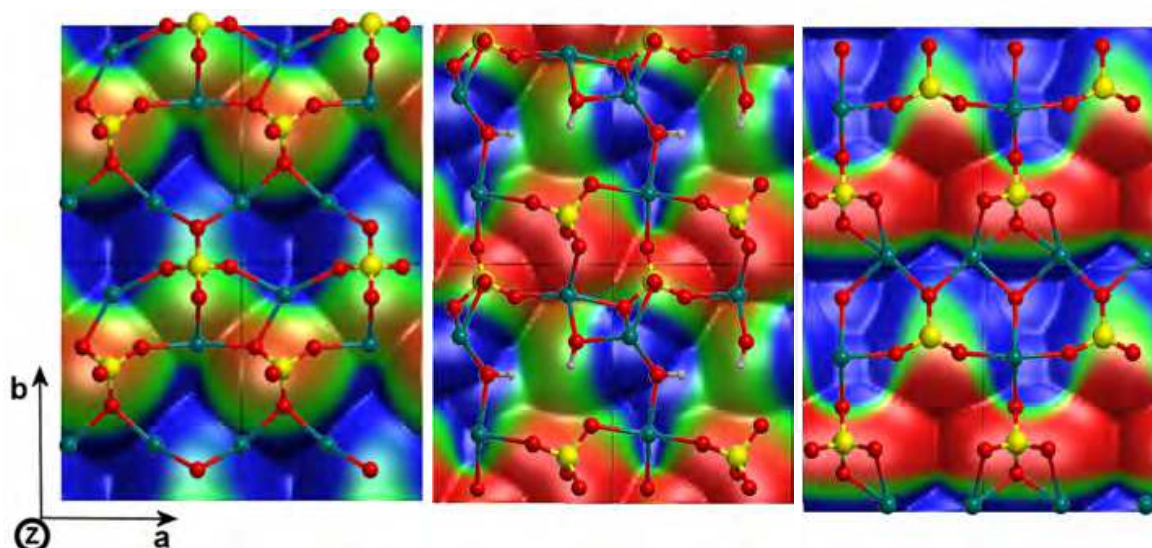


Fig. 3. Upper views of the three (010) surfaces: on the left side, the stoichiometric surface, in the middle, the Ca-rich surface and, on the right side, the P-rich surface. Each structure is superimposed on an isodensity surface colorcoded with the electrostatic potential (blue is most positive, red is most negative). The maps have been generated with the VMD program (Humphrey, Dalke & Schulten, et al., 1996). Calcium represented in cyan, oxygen in red, hydrogen in grey and phosphorous in yellow.

where A is the surface area (doubled, because two faces are generated), E_{bulk} and E_{slab} are the calculated energies of the related models and n is an integer number, required to match the chemical potentials of the two systems. Astala and Stott adopted a clever and rather involved scheme to evaluate the phase existence conditions for the two non-stoichiometric surfaces, showing that the region of their stability is outside the stability window defined by bulk HA, $\text{Ca}(\text{OH})_2$ and $\beta\text{-Ca}_3(\text{PO}_4)_2$ (Astala & Stott, 2008).

The typology of the exposed layers differentiates the (010) stoichiometric surface from the non-stoichiometric ones. Indeed, the (010) Ca-rich surface exposes the OH^- ions belonging to the B layer, while both the stoichiometric and the P-rich surfaces contain the OH^- ions in an inner layer (see the structures displayed in Fig. 3 for details).

| | Stoichiometric | Ca-rich | P-rich |
|------------------------|---------------------|---------------------|---------------------|
| a (Å) | 6.98 | 6.93 | 7.00 |
| b (Å) | 9.28 | 9.27 | 9.33 |
| γ (°) | 89.87 | 90.01 | 90.02 |
| Area (Å ²) | 64.83 | 64.24 | 65.24 |
| * Thickness (Å) | 13.28 | 20.05 | 20.23 |
| <Ca-O> (Å) | 2.41 | 2.39 | 2.40 |
| <P-O> (Å) | 1.55 | 1.55 | 1.55 |
| <O-H> (Å) | 0.97 | 0.97 | 0.97 |
| <OPO> (°) | 109.5 | 109.4 | 109.4 |
| Band Gap (eV) | 6.21 | 6.80 | 6.65 |
| Dipole (Debye) | $3.5 \cdot 10^{-3}$ | $4.0 \cdot 10^{-3}$ | $1.4 \cdot 10^{-2}$ |

* The slab thickness is the perpendicular distance between the most exposed Ca ions on the upper and lower faces of the slab.

Table 1. Most important geometrical parameters of the HA (010) surfaces. The values in <...> correspond to the arithmetical averages of the considered feature.

In Fig. 3, the most exposed layers of the three terminations are reported, superimposed on the isodensity surface colorcoded with the electrostatic potential. The isodensity value is fixed to 10^{-6} electrons and the electrostatic potential spans from -0.02 a.u. (red) to +0.02 a.u. (blue). Positive values of the potential are visible in correspondence of the Ca ions while negative potential zones are mostly located upon superficial phosphate ions.

In Table 1, a geometrical analysis of the three surfaces is reported. The cell parameters are slightly different between the three cases, but the rectangular shape is mostly maintained. The slab thickness is not comparable, because of a different number of layers for each surface model. The interatomic distances and angles are, however, very similar.

Two important intensive parameters can classify the stability of a slab structure, the electronic band gap and the total dipole moment across the slab: each surface has a dipole moment close to zero and a band gap typical of electrical insulators. The three surfaces are, then, stable and can be adopted as a substrate to study the adsorption of molecules.

2.1.2 Adsorption of H₂O and CO upon the most exposed Ca ions of the (010) surfaces

The chemical reactivity of the most exposed cations of a surface is experimentally studied with the IR technique by monitoring the perturbation of the vibrational frequency of the probe molecule, which is compared to the value for the free molecule. Of the possible probe

molecules, those commonly used are carbon monoxide and water, because of their selectivity towards cations, the ease of interpretation of their spectra, and the high sensitivity of IR instrumentation in the region where their vibrational frequencies fall (medium IR). The (010) stoichiometric surface has already been fully characterized by Corno *et al.* in relation to the adsorption of these molecules (Corno *et al.*, 2009), whereas the non-stoichiometric surfaces are the subject of this work. Calculations provide binding energies and vibrational frequencies of the probe molecules which can be used as a future reference to be compared with experimental measurements. In Fig. 4, the optimized structures of the adducts are reported for water and CO.

The adsorptions of water upon the most exposed cations of the non-stoichiometric surfaces are characterized by BE values of 131 and 125 kJ/mol (BSSE \approx 35 %), for the Ca-rich and P-rich surfaces, respectively. These values also take into account the formation of two hydrogen bonds between the water molecule and exposed anions, either phosphate only, or also hydroxyl anions in the case of the (010) Ca-rich surface. If the thermal and vibrational contributions are taken into account, these values decrease to 117 and 110 kJ/mol, respectively, allowing a consistent comparison with the experimental differential heat of adsorption of water of 110 kJ/mol (Corno *et al.*, 2009). The latter value has been obtained from experimental micro-calorimetric studies of water adsorption on microcrystalline HA, for a loading of water comparable with our models.

The adsorption of CO upon the most exposed Ca ions gives results highly representative of the strength of the cationic site as no hydrogen bond can be formed: the BE values upon the Ca-rich and P-rich surfaces are, respectively, 38 and 40 kJ/mol (BSSE \approx 20 %), showing an almost equivalence for the two Ca ions for the two surfaces.

When the vibrational features are considered, a crucial point is the comparison between the frequencies of the free and the adsorbate molecule. While the stretching mode of CO is easily identified in both cases, the modes of the adsorbed water molecule are no longer easily referable to those of the free molecule. The free water molecule is characterized by two stretching modes (the symmetric and, at higher frequencies, the anti-symmetric) and one bending mode. When the molecule interacts with the surface, these two kinds of stretching modes are no longer classifiable on a symmetry ground. The hydrogen bonds which are formed with the most exposed anions of the surface cause the loss of the C_{2v} symmetry of the molecule: each OH bond oscillates independently. As in previous work, we decided to compare the lower OH stretching frequency of the adsorbed molecule to the symmetric mode and *vice versa* (Corno *et al.*, 2009).

With these remarks, the calculated symmetric stretching shifts are -761 and -329 cm^{-1} for the (010) Ca-rich and (010) P-rich surfaces, respectively, while the anti-symmetric shifts are -310 and -328 cm^{-1} . The shifts of the bending frequencies are 113 and 88 cm^{-1} . When a hydrogen bond pattern occurs, the stretching mode shifts are negative due to the electronic density transfer and the resulting decrease of the bond strength. Instead, the bending frequencies increase because of the restraint caused by the hydrogen bond itself. The larger shift of the symmetric stretching of the H_2O adsorbed on the (010) Ca-rich surface, in combination with a larger bending shift, indicates the formation of a very strong hydrogen bond with an exposed anion of the (010) Ca-rich surface. Experimentally, the shift of the stretching is -400 cm^{-1} while the bending shift is 40 cm^{-1} . The calculated values are, then, in agreement with the experimental ones as long as the signs and the trends are considered (Bertinetti *et al.*, 2007).

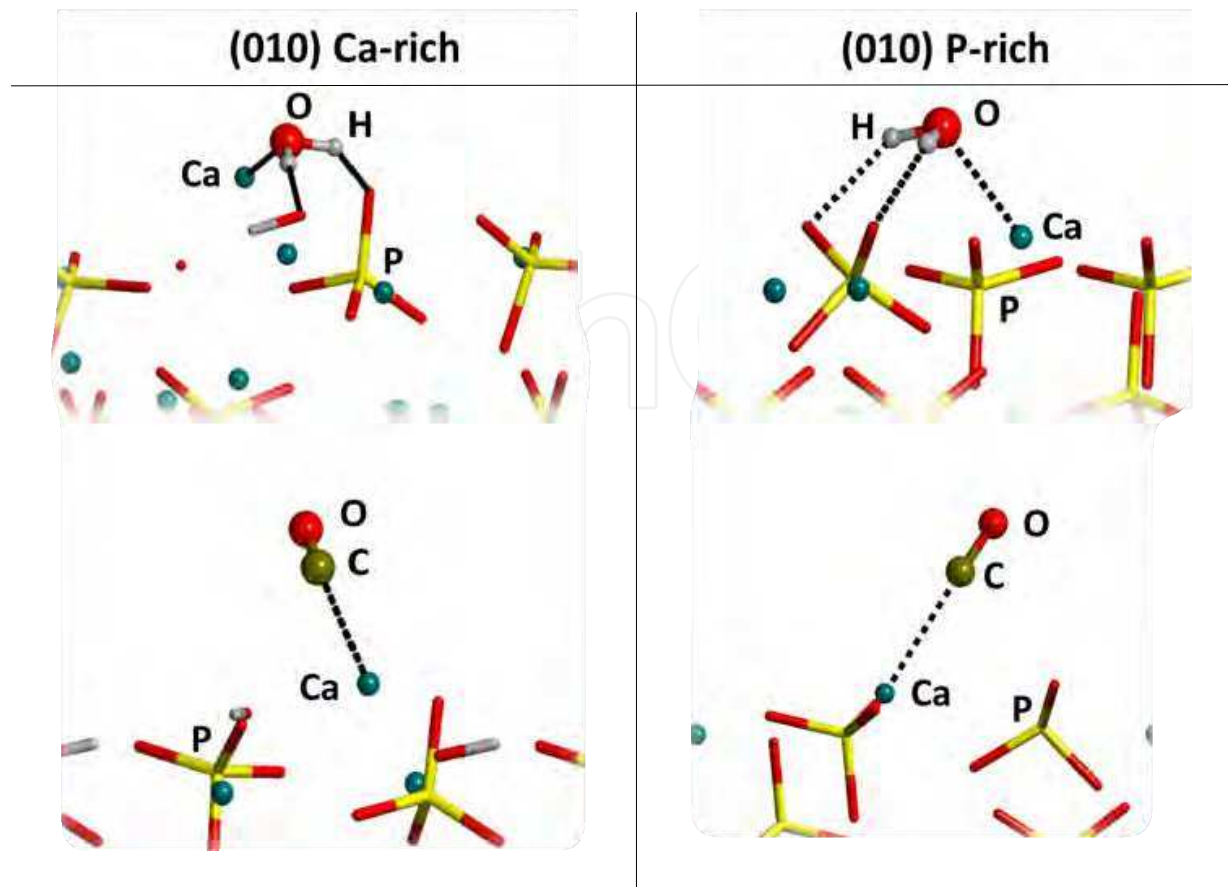


Fig. 4. Best views of the interactions between the most exposed ions of the (010) Ca-rich and (010) P-rich surfaces and the two probe molecules, water and carbon monoxide. The interactions with Ca ions and the hydrogen bonds are represented with dotted lines.

The stretching frequency shifts of the CO molecule are 40 cm^{-1} for the (010) Ca-rich surface and 41 cm^{-1} for the (010) P-rich surface. These BE and frequency shifts values indicate that the Ca ion can reasonably be considered as the major cause of the activity of HA towards polar molecules free from H-bond interactions.

A comparison with the experimental IR spectrum of CO adsorbed on HA reveals two main components, characterized by an upward shift of the stretching frequency of the adsorbed molecule of about $+27$ and $+41\text{ cm}^{-1}$, respectively. The highest shift is attributed to a tiny fraction of the most exposed calcium ions, which are those modeled in our studies, so proving a good agreement. On the other hand, the majority of calcium sites contribute to the lowest shift (Bertinetti et al., 2007; Sakhno et al., 2010).

2.1.3 Hydroxyapatite and carbonate ion defects

HA is the main component of the inorganic phase of bones and teeth, but, as many studies have demonstrated, the mineral present in those tissues is neither crystalline nor without defects (Fleet & Liu, 2003; Fleet & Liu, 2004; Fleet & Liu, 2007; Rabone & de Leeuw, 2005; Astala & Stott, 2005; Astala et al., 2006; Rabone & de Leeuw, 2007; de Leeuw et al., 2007). Indeed, it incorporates many other elements, ions or compounds, such as Mg or other alkaline earth metals instead of Ca, and, above all, the carbonate anion. Many studies, both theoretical and experimental, have already been conducted on the role of the carbonate ion

on the hydroxyapatite structure, in order to comprehend where and how this ion is located. The results of these studies assert that the CO_3^{2-} can substitute an OH^- ion of the structure, a *type A* defect, or a PO_4^{3-} , a *type B* defect. This hypothesis has been confirmed by IR spectra in which the vibrational mode frequencies of the carbonate are different for each type of substitution.

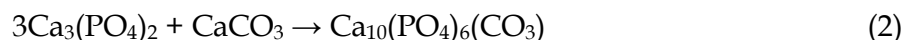
As the net charge of the carbonate is different from those of the substitutional anions, charge compensation is required.

In the case of the type A defect, the charge excess can be compensated by creation of an ionic vacancy removing another OH^- ion, also because of the larger steric encumbrance of the carbonate ion with respect to the hydroxyl ion (Peroos et al., 2006).

In the case of the type B defect, the electro-neutrality can be maintained in five different ways (Astala & Stott, 2005):

1. Removal of one OH^- ion and creation of one Ca vacancy (B1 complex);
2. Removal of one Ca ion for every two carbonate ions (B2 complex);
3. Substitution of one Ca with one hydrogen (B3 complex);
4. Substitution of one Ca with one alkaline ion;
5. OH^- ion incorporation close to the carbonate ion.

When considering the type A defect, it is first necessary to notice that, in the hydroxyapatite unit cell, only two OH^- ions are present (Fig. 1). If they are both removed at once but only one carbonate ion is included, the resulting structure is no longer a hydroxyapatite, as it had lost all the hydroxyl ions, and has to be considered a carbonated apatite. In Fig. 5, this stable structure is reported. The similarity between carbonate apatite and calcite structures is clear: the averaged distance $\langle \text{Ca-OC} \rangle$ is 2.35 Å in the carbonate apatite and 2.34 Å in the calcite. From the *ab initio* calculation, it is also possible to predict the enthalpy of formation of the carbonate apatite from the calcium phosphate and the calcite structures, considering the reaction (2):



The B3LYP enthalpy of formation is -35 kJ/mol, directly comparable with the value of -32 kJ/mol obtained with the VASP code and the PW91 functional (Rabone & de Leeuw, 2007).

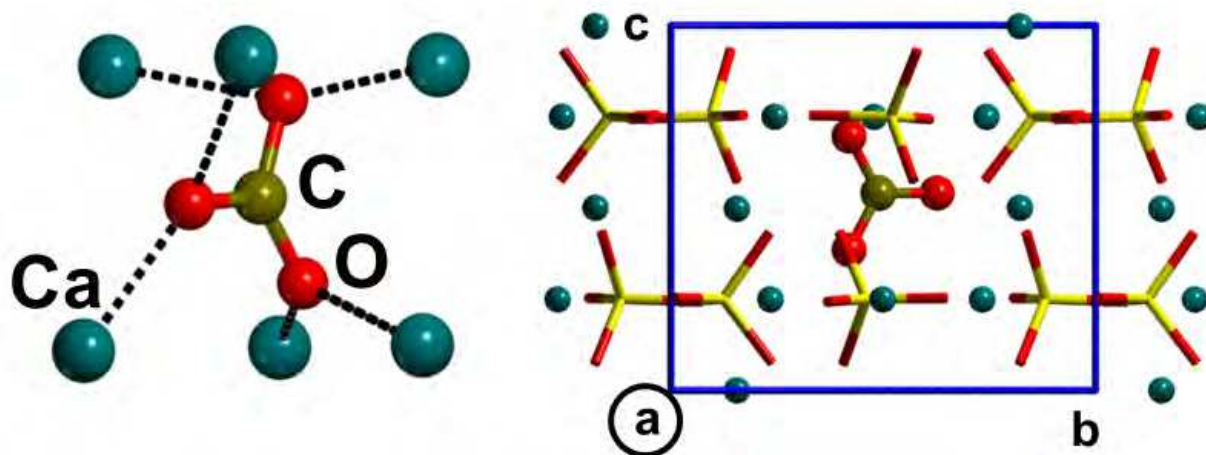
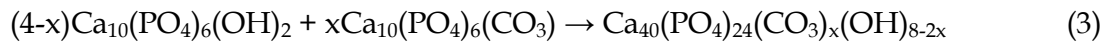


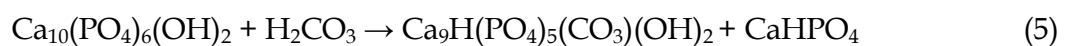
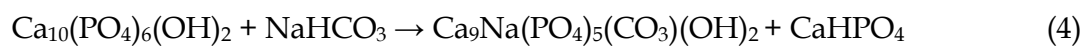
Fig. 5. Carbonated apatite. On the left side, a view of the carbonate ion is reported, highlighting its distances to the closest Ca ions. On the right side, the cell, where both OH^- are removed and one carbonate is substituted, is reported after full relaxation of the atoms.

As the main interest in the type A defect is the stability of the OH-CO₃²⁻ substitution as a function of CO₃²⁻ content, we modeled three cases using a 2x2 supercell:



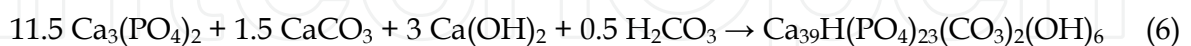
The most stable case occurs (see Fig. 6A) when three out of four pairs of OH ions ($x=3$) were substituted with carbonate ions ($\Delta E_r = -24$ kJ/mol). It is notable that the percentage of carbonate related to this minimum energy structure (4.4%) is close to that found in dentine tissue (5.6%) and in tooth enamel (3.5%) (Dorozhkin, 2009).

Among the five typologies of B type defect, we investigated only the substitution of Ca with Na or H. As all the phosphate ions are equivalent by symmetry, the substitution with carbonate is easy. On the contrary, in the cationic substitution to restore the neutrality, there is a choice among ten Ca ions. These are not equivalent, as the symmetry is broken by the carbonate substitution. We selected only four Ca ions, those nearest to the carbonate, because from the experiment it is known that the two defective substituents are close to each other. Indeed, in the four selected cases, the most stable structures are those in which the distance between the substituents is minimum. The different stabilities were obtained by calculating the energy variation (ΔE_r) for the following reactions:



The ΔE_r is 108 kJ/mol for reaction (4) and -94 kJ/mol for reaction (5), indicating that the inclusion of H is much more preferable than Na. The reason relies upon the formation of bulk water between the H and the OH ion of the column. This water molecule stabilizes the structure and its removal requires 136 kJ/mol, because of the occurrence of rather strong H-bonds. The two structures are reported in Fig. 6 (B/Na and B/H).

We also calculated some bulk structures in which both typologies (A and B) of substitutions were present at the same time, in order to better mimic the bone features. Among all the simulated structures, the most favorable situation is the one reported in Fig. 6 (A+B/H): a carbonate ion substitutes a pair of OH ions while another carbonate replaces a phosphate with formation of a water molecule. The hydrogen bonds formed by the water molecule are stronger than those of the B defect model, highlighting that the two defects interact and influence each other. The energy of formation of the mixed A+B/H structure is -752 kJ/mol for the reaction 6.



2.2 Bioglass: the effect of varying phosphorous content

As already described in the Introduction of this Chapter, bioactive glasses are extensively studied as prostheses for bone and tooth replacement and regeneration. In particular, the 45S5 composition has continuously been investigated, not only in its compact form, whose applications are limited to low load-bearing, but also as particulates and powders for bone filler use. Hence, the computational investigations of the variation in composition for the different glass components still represent a very interesting and stimulating task.

In the computational area, the most natural method to simulate glassy materials is usually classical molecular dynamics via the melt-and-quench procedure. Recently, much

theoretical research work has been carried out on bioglasses using *ab initio* molecular dynamics, though the transferability of empirical potentials remains a challenging goal, typical of classical techniques (Tilocca, 2010).

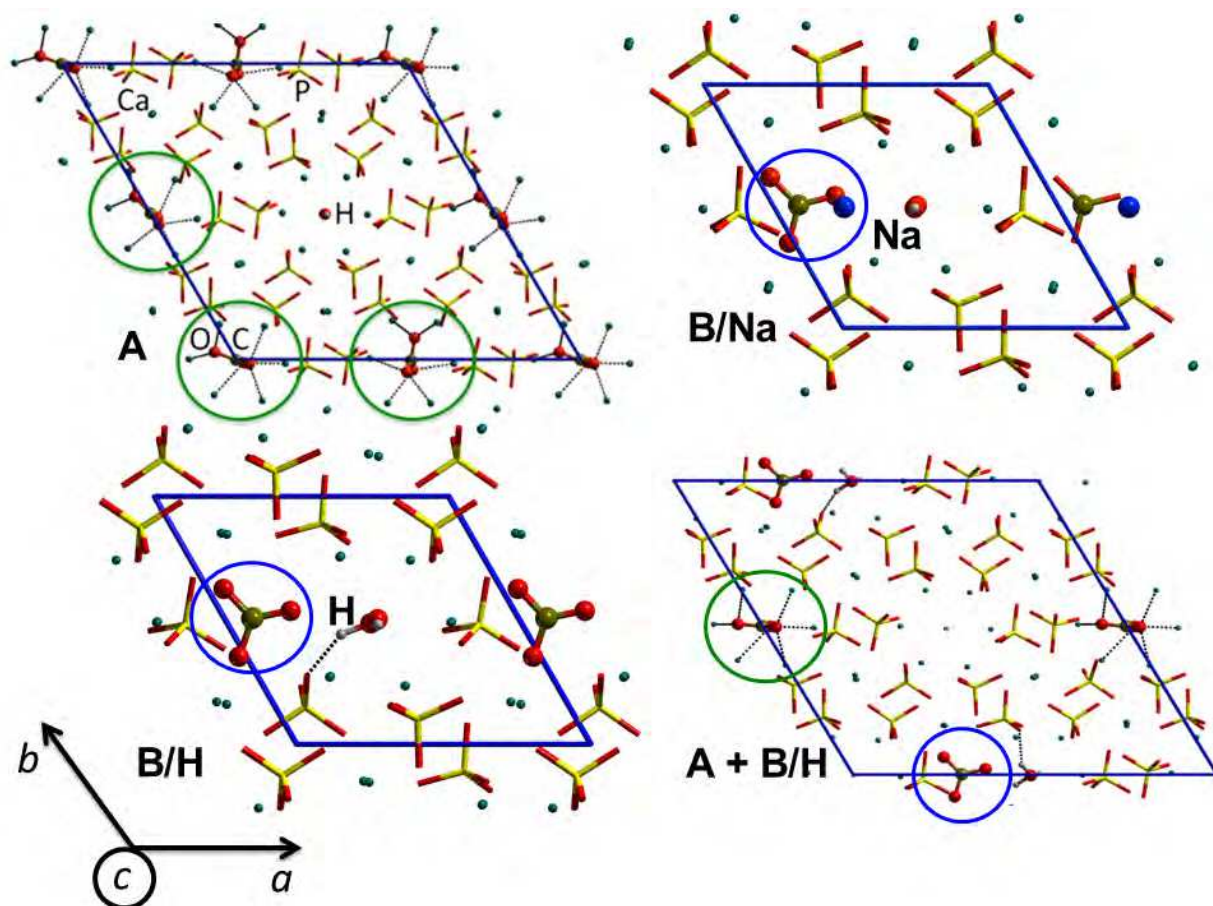


Fig. 6. Top views of the most stable carbonated hydroxyapatite structures. The carbonate can substitute a pair of hydroxyl ions (green circles) or a phosphate ion (blue circles). Top left, type A defect with three out of four pairs of OH ions substituted; top right, type B defect with Na as charge compensator; bottom left, type B with H as charge compensator; bottom right, type A and B, with H as charge compensator of the B type.

2.2.1 Multi-scale strategy for the modelling of 45S5 Bioglass®

The *ab initio* modelling of an amorphous material as the 45S5 Bioglass® has straightway caused a number of challenges. As the internal coordinates are not available from classical structural analysis, we have developed a multi-scale strategy to obtain a feasible amorphous bioglass model similar in composition to the 45S5. This approach has been largely illustrated in previous papers (Corno & Pedone, 2009; Corno et al., 2008; A. Pedone et al., 2008) so that here we only summarize the most important steps.

Firstly, we adopted classical molecular dynamics simulations to model a glassy bulk structure which could be close to the 45S5 composition keeping the size of the unit cell small enough for *ab initio* calculations, *i.e.* 78 atoms. In order to reproduce the correct ratio between SiO₂, P₂O₅, Na₂O and CaO components, the experimental density of 2.72 g/cm³ has been maintained fixed in a cubic box of 10.10 Å per side. After randomly generating atomic

positions, a melt-and-quench procedure was simulated: heating at 6000 K and then equilibrating for 100 ps. Next, continuously cooling from 6000 to 300 K in 1140 ps with a nominal cooling rate of 5 K/ps was performed. The temperature was decreased by 0.01 K every time step using Nose-Hoover thermostat with the time constant parameter for the frictional coefficient set to 0.1 ps (Hoover, 1985). Simulations were carried out in the constant volume NVT ensemble and 100 ps of equilibration at constant volume and 50 ps of data production were run at 300 K. On the derived structures, static energy minimizations were carried out at constant pressure and volume and the most representative model was chosen for *ab initio* calculations.

The final candidate structure was minimized both in terms of internal coordinates and lattice parameters, performing full relaxation runs. In Figure 7a the quantum-mechanical optimized structure of the selected Bioglass model is displayed. In the unit cell, which has become triclinic due to the lattice parameter deformation, two phosphate groups are present: one isolated (orthophosphate) and the other linked to one silicon atom. The structural analysis was followed by the simulation of the IR spectrum. Figure 7b reports the comparison between experimental (Lusvardi et al., 2008b) and computed spectra, which shows a very good agreement between the two spectra. The punctual assignment of each peak in the simulated case has been published in a previous paper (Corno et al., 2008), where the 45S5 model has been compared with an amorphous silica structure, to investigate the role of network modifier cations and phosphate groups in structural and vibrational properties of a pure SiO₂ framework. Hence, the reliability of the chosen multi-scale strategy has been proved.

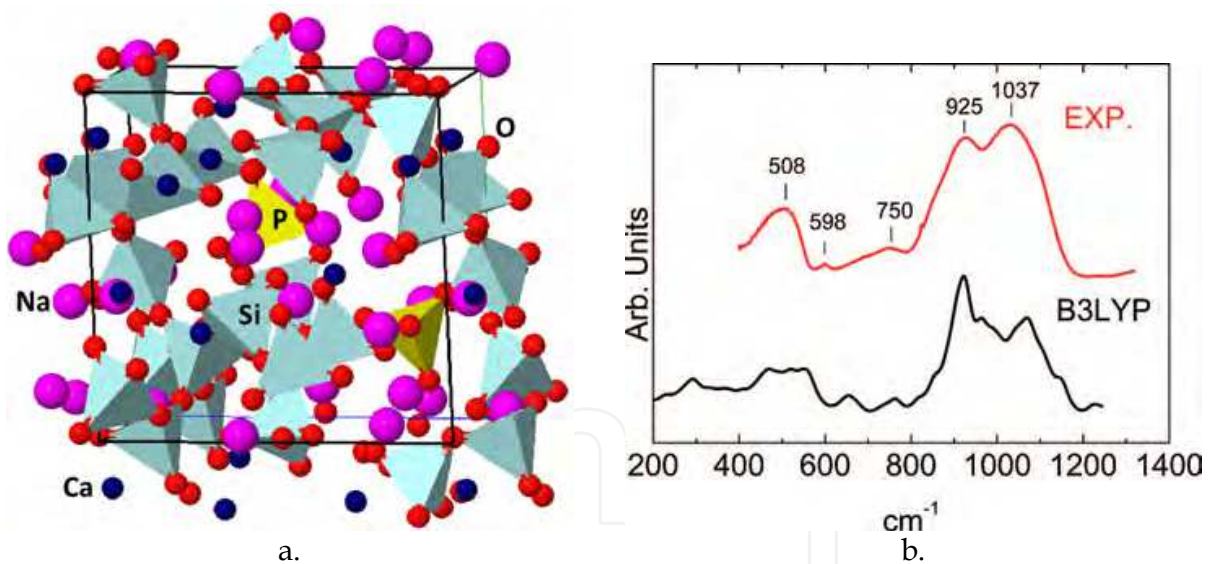


Fig. 7. 45S5 Bioglass model: a. best view of the optimized structure ($\text{Na}_{12}\text{Ca}_7\text{P}_2\text{Si}_{13}\text{O}_{44}$ composition), colour coding: silicon light blue, oxygen red, sodium pink, calcium dark blue and phosphorous yellow; cell parameters drawn in red for *a*, in green for *b* and in blue for *c*, while cell borders are in black; b. experimental (red line) and B3LYP (black line) IR spectra. (Corno et al., 2008; Lusvardi et al., 2008b)

2.2.2 Simulation of bioactive glasses with different P₂O₅ content

More recently, the influence of P₂O₅ content on the structure of bioactive glass compositions has been object of investigation (O'Donnell et al., 2009; O'Donnell et al., 2008a; O'Donnell et

al., 2008b). Indeed, it is well known that structural and compositional features of bioactive glasses are strongly connected to their bioactivity (Clayden et al., 2005; Lin et al., 2005). In particular, it has been demonstrated (Tilocca, 2010) that in compositions less bioactive than the 45S5 the majority of phosphate groups are linked to one or two silicon atoms. Conversely, in bioactive glasses as the 45S5, almost all the phosphate groups are isolated and mobile (Tilocca & Cormack, 2007).

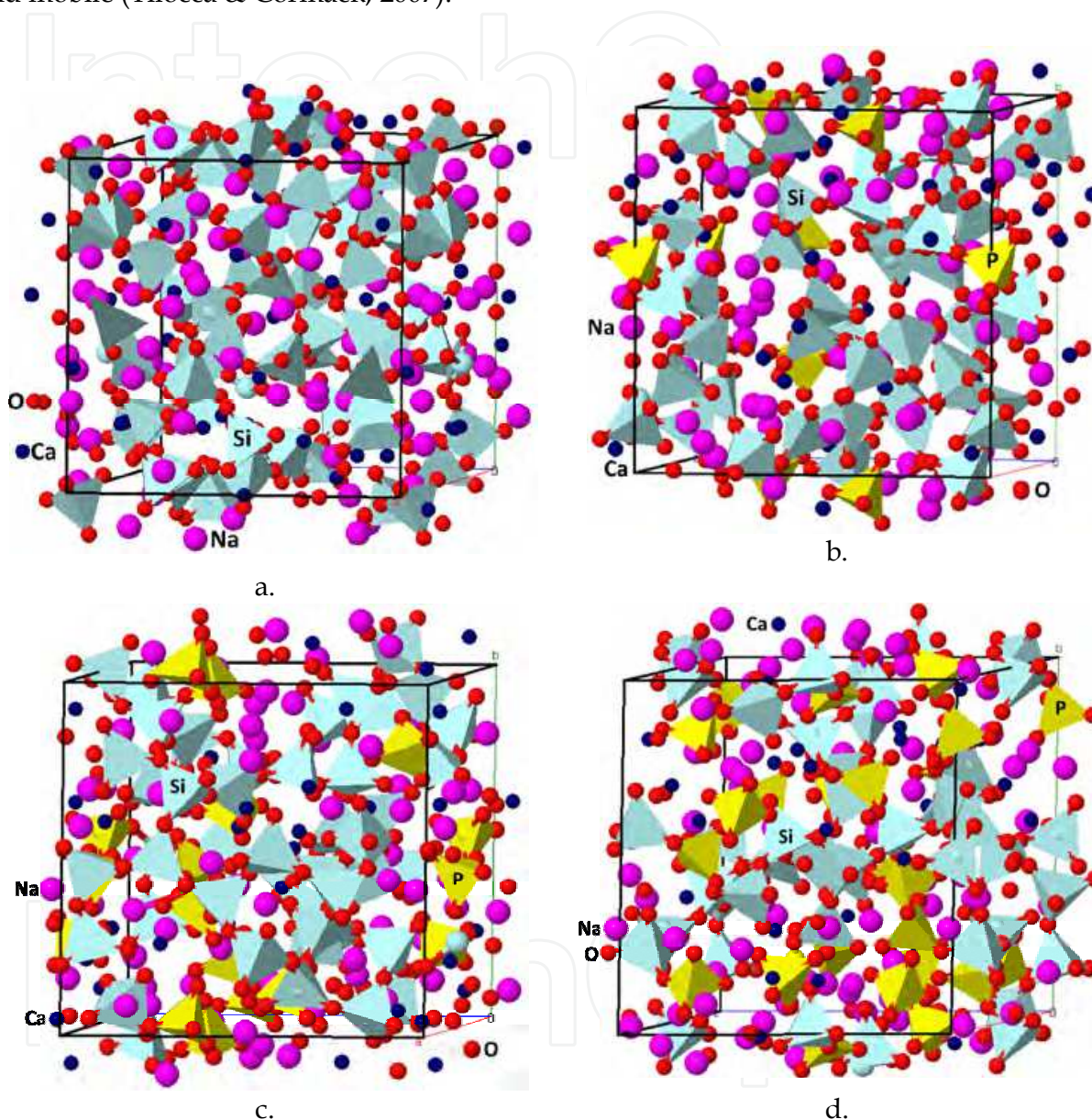


Fig. 8. Best views of the optimized structures of the four studied glass models: a. no phosphorous (P0); b. 2.5% phosphorous (P2.5); c. 5.5% phosphorous (P5.5) and d. 9.5% phosphorous (P9.5). Colour coding: silicon light blue, oxygen red, sodium pink, calcium dark blue and phosphorous yellow. Cell parameters drawn in red for *a*, in green for *b* and in blue for *c*, while cell borders are in black (their values listed in Table 5).

In our research work, we have aimed to correlate the change in phosphorous content with the change in structural and vibrational properties, these latter as a tool to detect the local

coordination of the PO_4 group. To this extent, four models of phosphate soda-lime glasses were studied by applying the same melt-and-quench procedure used for the 45S5 Bioglass®. The unit cell size has also been increased from the former 78 atoms to new models containing an average of 250 atoms. The larger size has allowed us to derive models which could be more representative of the amorphous long-range disorder typical of glassy materials.

The main structural features of the four modelled structures, whose correspondent images are displayed in Figure 8., are listed in Table 2, together with their molar composition. The “P0” structure refers to a phosphorous-free soda-lime glass.

| Model | SiO ₂ | CaO | Na ₂ O | P ₂ O ₅ | <i>a</i> | <i>b</i> | <i>c</i> | α | β | γ | Volume |
|-------|------------------|-----|-------------------|-------------------------------|----------|----------|----------|----------|---------|----------|--------|
| P0 | 45 | 24 | 22 | - | 14.97 | 14.23 | 14.77 | 91.3 | 90.7 | 89.2 | 3144 |
| P2.5 | 41 | 23 | 20.5 | 2.5 | 14.47 | 14.72 | 14.69 | 90.0 | 91.5 | 90.9 | 3128 |
| P5.5 | 35 | 23 | 20.5 | 5.5 | 14.68 | 14.47 | 15.08 | 91.4 | 90.0 | 87.9 | 3199 |
| P9.5 | 27 | 21 | 19.5 | 9.5 | 14.71 | 14.78 | 14.50 | 92.2 | 90.2 | 90.1 | 3150 |

Table 2. Molar per cent composition of the four studied models of glasses together with the unit cell parameter values of the optimized structures illustrated in Fig. 6. Lattice parameters expressed in Å, angles in degrees and volumes in Å³.

A direct comparison of volume values for the four models is not reasonable, since there are a number of tiny differences in molar composition in order to maintain the desired ratios between components as well as the total electroneutrality. Indeed, no linear relationship exists between the increase in %P₂O₅ and volume.

A comparison between the structural and vibrational features of the two models mostly similar in composition to the 45S5 Bioglass® has been carried out, *i.e.* the unit cell with 78 against that with 248 atoms (P2.5 of Figure 8b). In the smaller structure, as already described and illustrated in Figure 7, two phosphate groups are present: one isolated and the other connected to the silicon framework. In the larger model, five phosphate groups are located inside the unit cell, three of which are isolated, while the others linked to the siliceous network. In terms of Qⁿ species (a Qⁿ species is a network-forming ion, like Si or P, bonded to *n* bridging oxygens), the 60% of the total number of PO₄ groups is represented by Q⁰ (orthophosphates), while the remaining 40% is equally divided among Q¹ and Q² (see Figure 9b, blue curve). If we analyse the total radial distribution function *g*(*r*) for the P2.5 model plotted in Figure 9a., it clearly appears by the two peaks that the bond length of the P-NBO bond (NBO stands for non-bridging oxygen) is slightly shorter than that for the P-BO bonds (1.552 compared to 1.616 Å, respectively). Moreover, the P-BO bonds are numerically much less, as visible from the part b. of the same Figure 9.

Considering the Qⁿ distribution for the other two phosphorous-containing models, namely P5.5 and P9.5, it results: for P5.5 the 73% of the total 11 phosphate groups are isolated while the rest are Q₁ and for the total 19 phosphate groups of the P9.5 model, 37% are isolated, 58% are Q₁ and the 5% Q₂, in other words 7 Q₀, 11 Q₁ and a Q₂. The graph in Figure 9a. schematizes the different distribution for the larger models.

The P-O bond distances, both for bridging and non-bridging oxygens, vary according to the different Qⁿ species, as reported in Table 3.

As a general comment, P-NBO distances follow the trend: Q⁰ > Q¹ > Q² while for P-BO values in case of Q¹ and Q² species there is no definite trend, probably due to the limited number of sites in the considered structures.

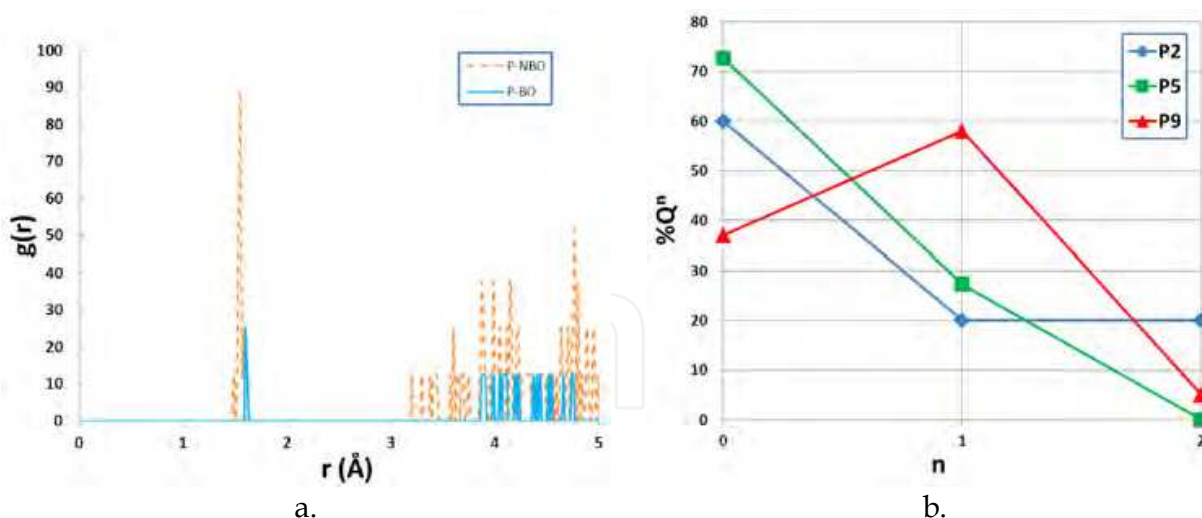


Fig. 9. a. Radial distribution function of the total P-O bonds, distinguishing between non-bridging oxygen (NBO, orange dotted line) and bridging oxygen (BO, blue line); b. percentage distribution of the phosphate groups in terms of Q^n species for the three large models P2.5 (blue), P5.5 (green) and P9.5 (red).

| Model | <P-NBO> Q^0 | <P-NBO> Q^1 | <P-NBO> Q^2 | <P-BO> Q^1 | <P-BO> Q^2 |
|-------|---------------|---------------|---------------|--------------|--------------|
| P2.5 | 1.556 | 1.539 | 1.508 | 1.597 | 1.602 |
| P5.5 | 1.559 | 1.523 | - | 1.660 | - |
| P9.5 | 1.557 | 1.531 | 1.515 | 1.631 | 1.588 |

Table 3. Average P-O bond lengths for both bridging and non-bridging oxygen of the three P2.5, P5.5 and P9.5 models are reported in Å.

2.2.3 Effect of P_2O_5 content on the simulated IR spectra

A complete vibrational analysis was outside our computational facilities, due to the size of the simulated bioglass models (250 atoms inside the unit cell, no symmetry). An alternative approach, here adopted, is the so-called “fragment” calculation of frequency. It consists on the selection of the interesting atoms – in this case phosphate groups – to be considered for the calculation of vibrational normal modes. Obviously this approach is an approximation and needs to be first tested. Our test case was the 45S5 structure of Figure 7a, for which the full IR spectrum was available. In particular for the phosphate groups containing Q^1 and Q^2 species, the question was to decide whether to include or not the linked silicon atom with or without its connected oxygen atoms.

Figure 10 reports three simulated IR spectra of the 45S5 model: the full spectrum (black line), the full spectrum including only modes involving phosphate groups (red line) and the partial spectrum where the fragment contains only phosphate groups and silicon atoms linked to the Q^1 species.

In order to dissect the contribution to the full IR spectrum (black spectrum, Fig. 10) of modes involving the displacements of P atoms we rely on the Potential Energy Distribution (PED). All modes involving the P atom in the PED of the full spectrum are included whereas the remaining ones are removed from the spectrum (red spectrum, Fig. 10). The comparison with the spectrum (blue spectrum, Fig. 10) computed by including as a fragment the PO_4 (for fully isolated groups) and $PO_4(SiO_4)_{1,2}$ (for the other cases) shows a good agreement

with the black spectrum, so that this methodology has been adopted to compute the spectra for the larger structures with variable P content. In other words, the differences in peaks between the red and the blue spectra of Figure 10 are due to the presence (blue line) or absence (red line) of the extra SiO_4 group.

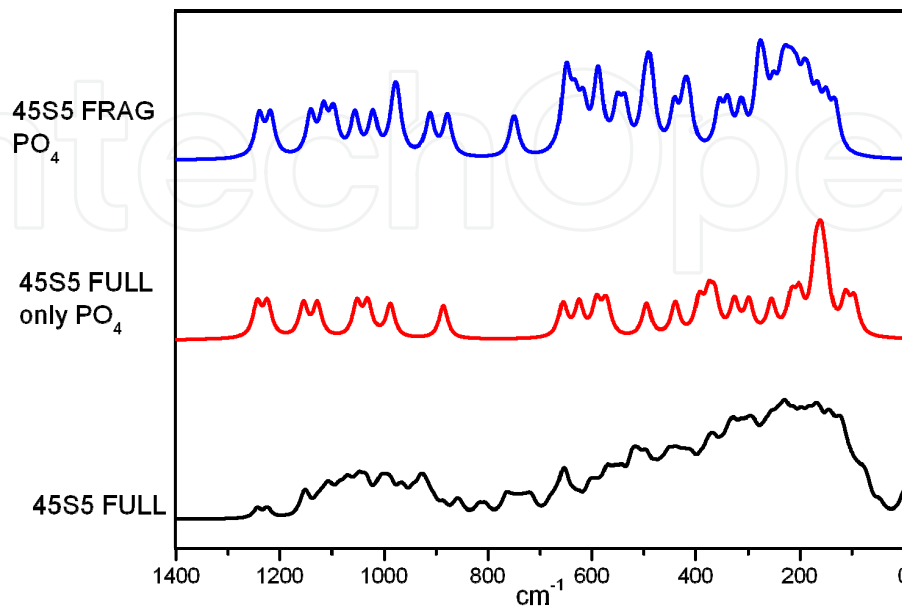


Fig. 10. Simulated IR spectra of the similar 45S5 Bioglass® model in the following sequence from bottom to top: full frequency calculation (black line), full frequency calculation including only PO_4 -involved modes (red line) and fragment calculation considering in the fragment PO_4 and SiO_4 which is directly bonded to PO_4 . No IR intensities are reported and the chosen band width is of 20 cm^{-1} .

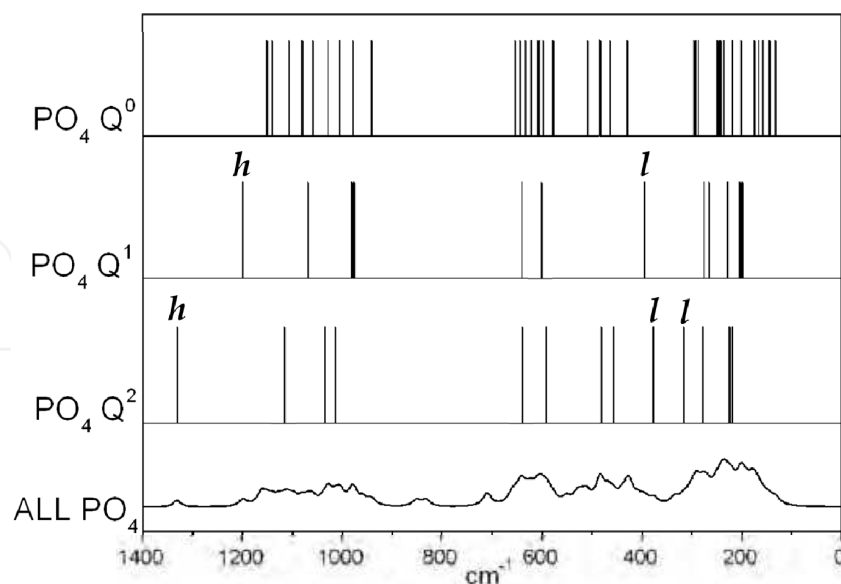


Fig. 11. IR peaks assignment for phosphate groups of the P2.5 model based on the different Q^n species. Label *h* and *l* refer to the peculiar bands at high and low frequencies, respectively, that allow us to distinguish the Q^0 species from the Q^1 and Q^2 . In case of Q_2 , see Fig. 12 for the schematic representation of the associated normal modes.

Figure 11 illustrates a specific example of how to detect the various phosphate groups in terms of Q^n (isolated or connected phosphates) by IR spectroscopy. We reported at the bottom of the graph the P2.5 IR spectrum of the phosphates computed applying the aforementioned procedure (fragment mode). The three bar charts refer each one to the Q^n species present inside the structure and show only the frequencies involving that specific class of phosphate groups (isolated or connected to the network). It is interesting to note the shift of the highest and lowest bands comparing Q^1 and Q^2 cases: the highest frequency – indicated with the label h – corresponds to the stretching of the P=O bond and is shifted to higher values in case of Q^2 , with respect to Q^1 and Q^0 . On the contrary, in the region of low frequencies, modes involving the Q^2 species are shifted to lower values compared to the Q^1 ones. The OPO bending region (600-700 cm^{-1}) remains almost unaffected.

Figure 12 illustrates the graphical representation of the normal modes displacement for the five stretching and bending modes of the Q^2 species present in the P2.5 glass.

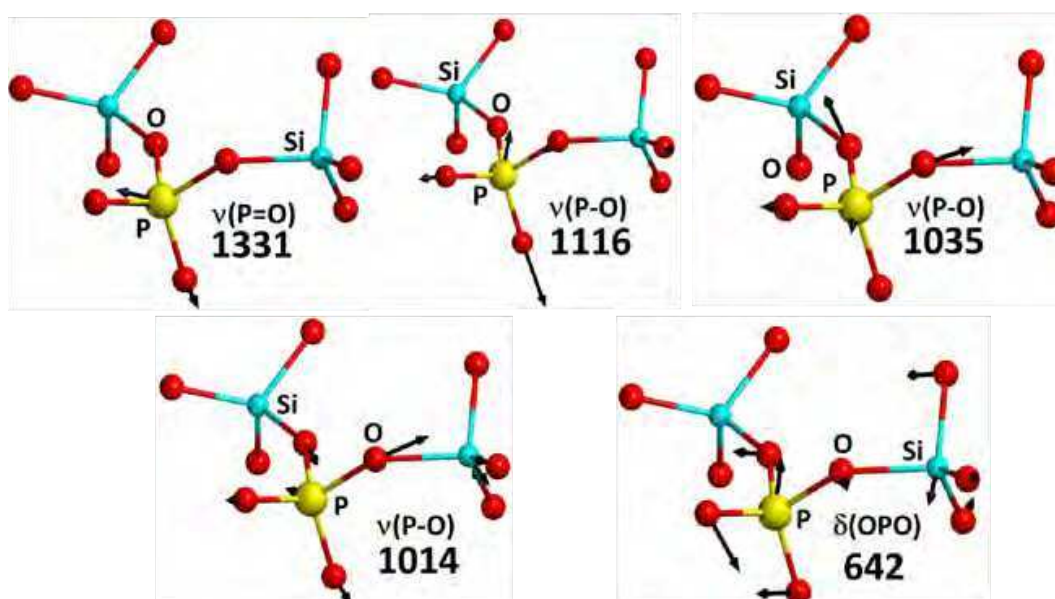


Fig. 12. Schematic representation of the normal mode displacement assigned to the Q^2 species for the P2.5 model (PO_4 structural unit connected to 2 SiO_4 groups). Colour coding: Si light blue, oxygen red, phosphorous yellow; frequencies expressed in cm^{-1} .

The simulated IR spectra for the phosphate groups of the three phosphorous-containing models have been then compared one to each other and to the phosphorous-free structure P0, as displayed in Figure 13.

The first evident difference between phosphorous-free P0 and the other models is the absence of bands in the spectral region at high frequencies (1200-1400 cm^{-1}). As we have discussed above, that is the typical region of the P=O stretching mode of phosphate groups. This mode is shifted to lower frequencies and the band is broadened when passing from P2.5 to P9.5. Another clear indication of the presence of phosphate groups is the band at about 600-700 cm^{-1} , which corresponds to the O-P-O bending region. The 1100-800 cm^{-1} spectral range, on the contrary, is not easily assigned to phosphate groups inside the bioglass since also Si-O stretching are located in that zone. However, the effect of increasing the P_2O_5 content inside the unit cell is reflected in a general broadening of the P-O stretching and O-P-O bending modes.

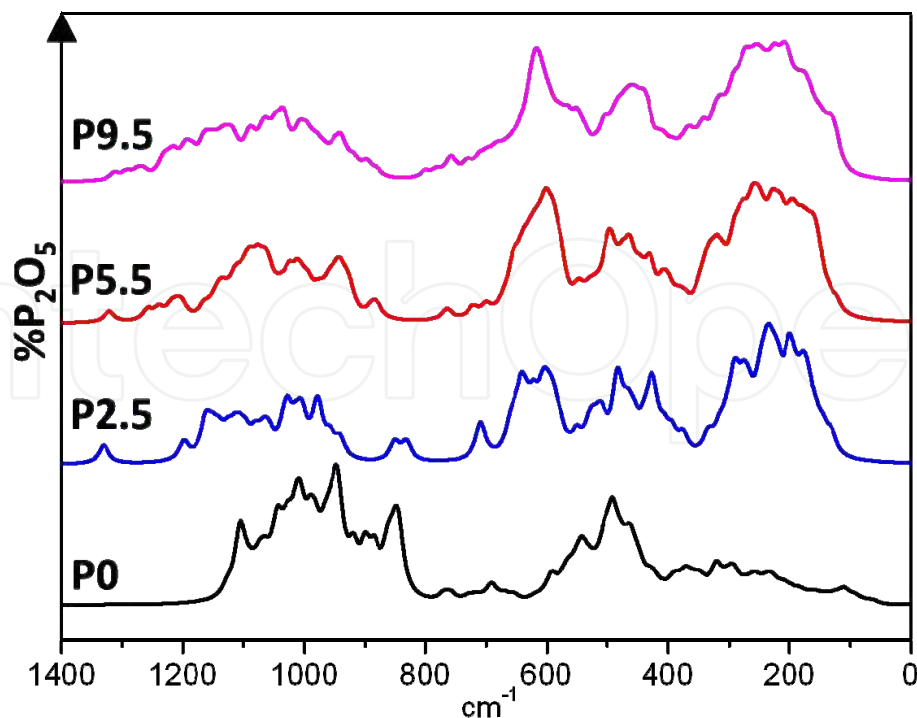


Fig. 13. Simulated IR spectra of the four models of glasses at increasing %P₂O₅ content.

2.2.4 Future perspectives: Surface modelling

The natural subsequent step in bioactive glass simulation deals with the modeling of surfaces. Indeed, each process of the Hench mechanism that leads to the implant integration typically occurs at the interface between the inorganic material and the biological fluid. Thus, the knowledge of surface properties, such as electrostatic potential and adsorptive behavior towards simple molecules as water, becomes essential in the investigation of bioglasses (Tilocca & Cormack, 2009).

Modeling surfaces is generally not a trivial task, particularly when the bulk material is amorphous. For an amorphous material the identification of a particular face by crystallographic indexes is rather arbitrary as the atomic density is statistically distributed in space in a rather uniform way. A second difficulty is the need of breaking both ionic and covalent bonds during the slab definition which may render the system non-neutral.

In Figure 14, the model of one of the many possible bioglass surfaces extracted from the P2.5 bulk of Figure 8b is presented. The surface was cut out from the bulk as a real 2D slab (infinite in the two dimensions), dangling bonds were saturated with hydrogen atoms and a full optimization run was performed. The resulting surface is very interesting per se, but much more considering its behaviour when hydrated, since water molecules are ubiquitously present in the biological fluids where the material is immersed. In particular, a key issue is to see whether H₂O will chemisorb by dissociating on the exposed Na⁺ and Ca²⁺ cations, a step essential in the Hench mechanism.

In our laboratory a systematic study of the several possible surfaces of the structure with the 45S5 composition is on-going. The application of different methodologies, such as *ab initio* molecular dynamics, already used in the literature (Tilocca, 2010), will be considered to fully characterize the adsorption processes of water and even collagen occurring at the interface between bioactive material and the biological tissue.

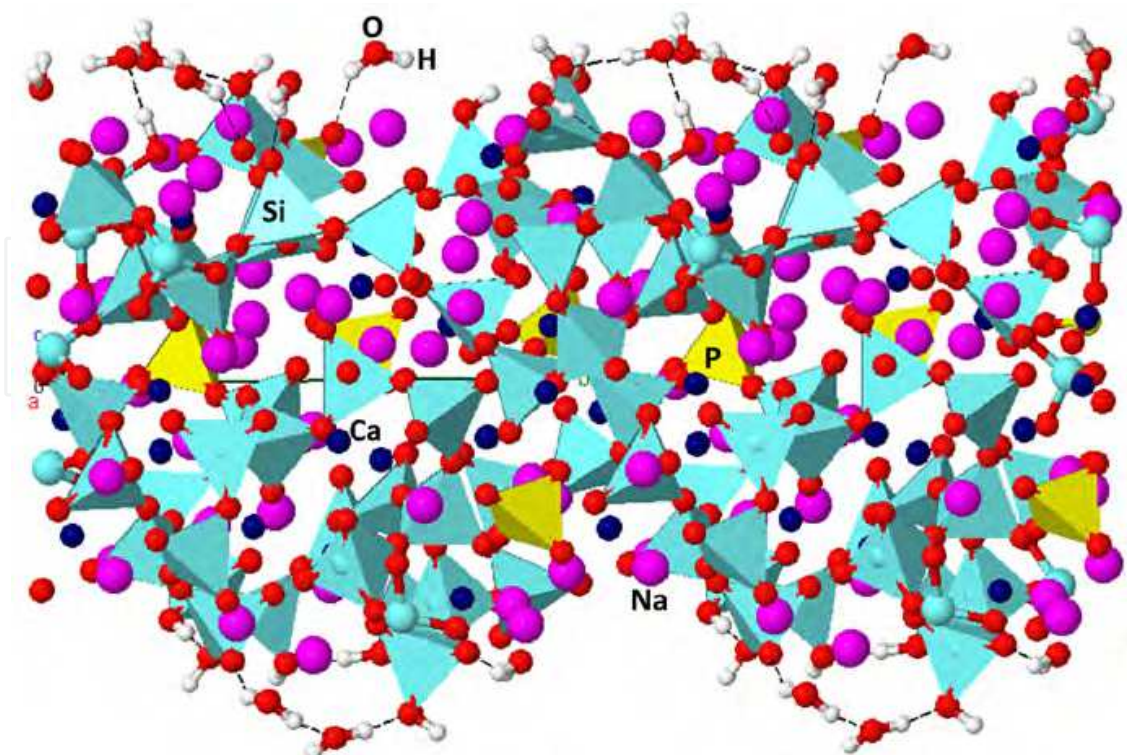


Fig. 14. Surface model of the P2.5 bioglass with adsorbed water molecules at both top and bottom faces. Colour coding: silicon light blue, oxygen red, sodium pink, calcium dark blue, phosphorous yellow, hydrogen bonds black dotted line.

3. Conclusion

In the present Chapter it has been explained how crucial the computational techniques are when applied together with experimentalist measurements in the understanding of biological complex systems and mechanisms dealing with biomaterials for a large number of reasons. Indeed, computational methods are extremely powerfully applied to predict structure formation and crystal growth as well as to describe at a molecular level the real interactions responsible of the attachment of the inorganic biomaterial to the organic tissue. In the investigation of phenomena related to a complex system such as the human body, many approximations are required, so a reductionist approach is employed also in the computational analysis.

In this Chapter, the approach has been explained for two typical biomaterials: hydroxyapatite and Bioglass® 45S5. In particular, for the first material, the aim was to describe the study of its (010) non-stoichiometric surfaces in interaction with water and carbon monoxide. For the latter, the adopted strategy has been analyzed and then a specific example has been reported, dealing with the spectroscopic characterization of computed vibrational features with the increasing amount of phosphorous in a sufficiently large unit cell starting from the well-know 45S5 Bioglass® composition.

The general knowledge gained in recent years through the use of computational techniques such as those described in this chapter is great, but not enough to fully understand the peculiar characteristics of the materials that make up the musculo-skeletal system and to provide appropriate care for important illnesses such as osteoporosis or degenerative and metabolic diseases, benign and malignant tumors and trauma.

To achieve this goal it is fundamental to understand the structure and properties of natural bone at a molecular level and to investigate the chemical-physical interaction between collagen and mineral phase comprising the bone composite.

This can only be achieved through the development and use of multiscale computational methods that combine quantum, classical and continuum approaches enabling to study chemical-physical-biological phenomena on large-scales both in space and time.

Regarding the study of the human bone, we believe that the key issues to be addressed by computational science researchers in the coming years will be the study of the structure and assembly of the collagen protein, the interaction at the molecular level of collagen with the mineral apatite, and finally the structure and mechanical properties of collagen-apatite composite.

As for the study of bioactive glasses, an important line of research that is developing in different research groups located in different nations involves the characterization of the chemical and physical properties and reactivity of the 45S5 Bioglass® surface. However, it will be wise not to neglect the study of the effect of composition on the structure and bioactivity of different systems and the study of the thermodynamics and crystallization kinetics of crystalline phases that are well-known to affect the bioactivity of the glass. Finally, the design of new bioactive glasses will also rely on a deep understanding of their fracture mechanism and the prediction of important properties such as brittleness and toughness, which determine the final use of glass.

4. Acknowledgment

The authors would like to thank the Distributed European Infrastructure for Supercomputing Applications (DEISA) for allowing of computational resources under the Extreme Computing Initiative (BIOGLASS Project). CINECA computing centre is also kindly acknowledged.

Colleagues V. Bolis (Dip. DiSCAFF, University of Eastern Piedmont) and G. Martra (Dip. Chimica IFM, University of Torino) are acknowledged for fruitful discussion and for providing the HA samples, synthesized and kindly supplied by ISTECC-CNR (Faenza, Italy).

R. Dovesi, B. Civalleri and the CRYSTAL team (Dip. Chimica IFM, University of Torino) are thanked for discussion and continuous support with the use of the code.

Part of the results on carbonated HA has been obtained by G. Ulian during his Master Degree Thesis, entitled "DFT study of carbonated defect in hydroxyapatite", 2010, University of Torino.

5. References

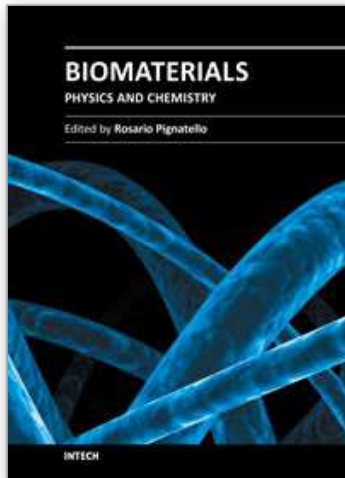
- Aina, V., Bonino, F., Morterra, C., Miola, M., Bianchi, C. L., Malavasi, G., Marchetti, M. & Bolis, V. (2011) Influence of the Chemical Composition on Nature and Activity of the Surface Layer of Zn-Substituted Sol-Gel (Bioactive) Glasses. *The Journal of Physical Chemistry C*, Vol.115, No.5, pp.2196-2210, ISSN 1932-7447.
- Astala, R. & Stott, M. J. (2005) First Principles Investigation of Mineral Component of Bone: CO₃ Substitutions in Hydroxyapatite. *Chemistry of Materials*, Vol.17, No.16, pp.4125-4133, ISSN 1520-5002.
- Astala, R. & Stott, M. J. (2008) First-principles study of hydroxyapatite surfaces and water adsorption. *Physical Review B*, Vol.78, No.7, pp.075427, ISSN 1550-235X.

- Astala, R., Stott, M. J. & Calderin, L. (2006) Ab Initio Simulation of Si-Doped Hydroxyapatite. *Chemistry of Materials*, Vol.18, No.2, pp.413-422, ISSN 1520-5002.
- Becke, A. D. (1993) Density-functional thermochemistry. III. The role of exact exchange. *The Journal of Chemical Physics*, Vol.98, No.7, pp.5648-5652, ISSN 0021-9606.
- Bertinetti, L., Tampieri, A., Landi, E., Ducati, C., Midgley, P. A., Coluccia, S. & Martra, G. (2007) Surface Structure, Hydration, and Cationic Sites of Nanohydroxyapatite: UHR-TEM, IR and Microgravimetric Studies. *The Journal of Physical Chemistry C*, Vol.111, No.10, pp.4027-4035, ISSN 1932-7447.
- Canepa, P., Chiatti, F., Corno, M., Sakhno, Y., Martra, G. & Ugliengo, P. (2011a) Affinity of hydroxyapatite (001) and (010) surfaces to formic and alendronic acids: a quantum-mechanical and infrared study. *Physical Chemistry Chemical Physics*, Vol.13, No.3, pp.1099-1111, ISSN 1463-9084.
- Canepa, P., Hanson, R. M., Ugliengo, P. & Alfredsson, M. (2011b) J-ICE: a new Jmol interface for handling and visualizing crystallographic and electronic properties. *Journal of Applied Crystallography*, Vol.44, No.1, pp.225-229, ISSN 0021-8898.
- Christie, J. K., Pedone, A., Menziani, M. C. & Tilocca, A. (2011) Fluorine Environment in Bioactive Glasses: Ab Initio Molecular Dynamics Simulations. *The Journal of Physical Chemistry B*, Vol.115, No.9, pp.2038-2045, ISSN 1520-6106.
- Clayden, N. J., Pernice, P. & Aronne, A. (2005) Multinuclear NMR study of phosphosilicate gels derived from POCl_3 and $\text{Si}(\text{OC}_2\text{H}_5)_4$. *Journal of Non-Crystalline Solids*, Vol.351, No.3, pp.195-202, ISSN 0022-3093.
- Corno, M., Busco, C., Bolis, V., Tosoni, S. & Ugliengo, P. (2009) Water Adsorption on the Stoichiometric (001) and (010) Surfaces of Hydroxyapatite: A Periodic B3LYP Study. *Langmuir*, Vol.25, No.4, pp.2188-2198, ISSN 1520-5827.
- Corno, M., Busco, C., Civalleri, B. & Ugliengo, P. (2006) Periodic *ab initio* study of structural and vibrational features of hexagonal hydroxyapatite $\text{Ca}_{10}(\text{PO}_4)_6(\text{OH})_2$. *Physical Chemistry Chemical Physics*, Vol.8, No.21, pp.2464-2472, ISSN 1463-9084.
- Corno, M., Orlando, R., Civalleri, B. & Ugliengo, P. (2007) Periodic B3LYP study of hydroxyapatite (001) surface modelled by thin layer slab. *European Journal of Mineralogy*, Vol.19, No.5, pp.757-767, ISSN 0935-1221.
- Corno, M. & Pedone, A. (2009) Vibrational features of phospho-silicate glasses: Periodic B3LYP simulations. *Chemical Physics Letters*, Vol.476, No.4-6, pp.218-222, ISSN 0009-2614.
- Corno, M., Pedone, A., Dovesi, R. & Ugliengo, P. (2008) B3LYP Simulation of the Full Vibrational Spectrum of 45S5 Bioactive Silicate Glass Compared to v-Silica. *Chemistry of Materials*, Vol.20, No.17, pp.5610-5621, ISSN 1520-5002.
- Corno, M., Rimola, A., Bolis, V. & Ugliengo, P. (2010) Hydroxyapatite as a key biomaterial: quantum-mechanical simulation of its surfaces in interaction with biomolecules. *Physical Chemistry Chemical Physics*, Vol.12, No.24, pp.6309-6329, ISSN 1463-9084.
- Currey, J. D. (1998) Mechanical properties of vertebrate hard tissues. *Proceedings of the Institution of Mechanical Engineers, Part H: Journal of Engineering in Medicine*, Vol.212, No.6, pp.399-411, ISSN 2041-3033
- de Leeuw, N. H., Bowe, J. R. & Rabone, J. A. L. (2007) A computational investigation of stoichiometric and calcium-deficient oxy- and hydroxy-apatites. *Faraday Discussions*, Vol.134, 195-214, ISSN 1364-5498.
- Dorozhkin, S. V. (2009) Calcium Orthophosphates in Nature, Biology and Medicine. *Materials*, Vol.2, No.2, pp.399-498, ISSN 1996-1944.
- Dovesi, R., Civalleri, B., Orlando, R., Roetti, C. & Saunders, V. R. (2005a). Ab Initio Quantum Simulation in Solid State Chemistry. In *Review in Computational Chemistry*, Vol. 21,

- K.B. Lipkowitz, R. Larter & T.R. Cundari (Ed.), pp. 1-127, John Wiley & Sons Inc., ISBN 9780471682394, New York
- Dovesi, R., Orlando, R., Civalleri, B., Roetti, C., Saunders, V. R. & Zicovich-Wilson, C. M. (2005b) CRYSTAL: a computational tool for the ab initio study of the electronic properties of crystals. *Zeitschrift fur Kristallographie*, Vol.220, No.5-6, pp.571-573, ISSN 0044-2968.
- Dovesi, R., Saunders, V. R., Roetti, C., Orlando, R., Zicovich-Wilson, C. M., Pascale, F., Civalleri, B., Doll, K., Harrison, N. M., Bush, I. J., D'Arco, P. & Llunell, M., CRYSTAL2009 User's Manual, Available from: <<http://www.crystal.unito.it>>
- Fleet, M. E. & Liu, X. (2003) Carbonate apatite type A synthesized at high pressure: new space group ($P-3$) and orientation of channel carbonate ion. *Journal of Solid State Chemistry*, Vol.174, No.2, pp.412-417, ISSN 1095-726X.
- Fleet, M. E. & Liu, X. (2004) Location of type B carbonate ion in type A-B carbonate apatite synthesized at high pressure. *Journal of Solid State Chemistry*, Vol.177, No.9, pp.3174-3182, ISSN 1095-726X.
- Fleet, M. E. & Liu, X. (2007) Coupled substitution of type A and B carbonate in sodium-bearing apatite. *Biomaterials*, Vol.28, No.6, pp.916-926, ISSN 0142-9612.
- Fratzl, P., Gupta, H. S., Paschalis, E. P. & Roschger, P. (2004) Structure and mechanical quality of the collagen-mineral nano-composite in bone. *Journal of Materials Chemistry*, Vol.14, No.14, pp.2115-2123, ISSN 0959-9428.
- Hench, L. (2006) The story of Bioglass®. *Journal of Materials Science: Materials in Medicine*, Vol.17, No.11, pp.967-978, ISSN 0957-4530.
- Hench, L. L. (1998) Biomaterials: a forecast for the future. *Biomaterials*, Vol.19, No.16, pp.1419-1423, ISSN 0142-9612.
- Hench, L. L. & Andersson, O. H. (1993). Bioactive glasses. In *An introduction to bioceramics*. In *An introduction to bioceramics*, L.L. Hench & W. J. (Ed.), pp. 42-62, World Scientific, ISBN 978-981-02-1400-5 Singapore.
- Hench, L. L., Splinter, R. J., Allen, W. C. & Greenlee, T. K. (1971) Bonding Mechanism at the Interface of Ceramic Prosthetic Materials. *Journal of Biomedical Materials Research A*, Vol.5, No.6, pp.117-141, ISSN 1552-4965.
- Hoover, W. G. (1985) Canonical dynamics: Equilibrium phase-space distribution. *Physical Review A*, Vol.31, No.3, pp.1695-1697, ISSN 1094-1622.
- Humphrey, W., Dalke, A. & Schulten, K. (1996) VMD: Visual Molecular Dynamics. *Journal of Molecular Graphics*, Vol.14, No.1, pp.33-38, ISSN 1093-3263.
- Levitt, S. R., Crayton, P. H., Monroe, E. A. & Condrate, R. A. (1969) Forming methods for apatite prostheses. *Journal of Biomedical Materials Research A*, Vol.3, 683-684, ISSN 1097-4636.
- Lin, C. C., Huang, L. C. & Shen, P. (2005) $\text{Na}_2\text{CaSi}_2\text{O}_6\text{-P}_2\text{O}_5$ based bioactive glasses. Part 1: Elasticity and structure. *Journal of Non-Crystalline Solids*, Vol.351, No.40-42, pp.3195-3203, ISSN 0022-3093.
- Lusvardi, G., Malavasi, G., Cortada, M., Menabue, L., Menziani, M. C., Pedone, A. & Segre, U. (2008a) Elucidation of the Structural Role of Fluorine in Potentially Bioactive Glasses by Experimental and Computational Investigation. *The Journal of Physical Chemistry B*, Vol.112, No.40, pp.12730-12739, ISSN 1520-6106.
- Lusvardi, G., Malavasi, G., Menabue, L., Menziani, M. C., Pedone, A., Segre, U., Aina, V., Perardi, A., Morterra, C., Boccafoschi, F., Gatti, S., Bosetti, M. & Cannas, M. (2008b) Properties of Zinc Releasing Surfaces for Clinical Applications. *Journal of Biomaterials Applications*, Vol.22, 505-526, ISSN 1530-8022.

- Matsumura, Y. & Moffat, J. B. (1996) Methanol adsorption and dehydrogenation over stoichiometric and non-stoichiometric hydroxyapatite catalysts. *Journal of the Chemical Society, Faraday Transactions*, Vol.92, No.11, pp.1981-1984, ISSN 0965-5000.
- O'Donnell, M. D., Watts, S. J., Law, R. V. & Hill, R. G. (2008a) Effect of P₂O₅ content in two series of soda lime phosphosilicate glasses on structure and properties - Part I: NMR. *Journal of Non-Crystalline Solids*, Vol.354, No.30, pp.3554-3560, ISSN 0022-3093.
- O'Donnell, M. D., Watts, S. J., Law, R. V. & Hill, R. G. (2008b) Effect of P₂O₅ content in two series of soda lime phosphosilicate glasses on structure and properties - Part II: Physical properties. *Journal of Non-Crystalline Solids*, Vol.354, No.30, pp.3561-3566, ISSN 0022-3093.
- O'Donnell, M., Watts, S., Hill, R. & Law, R. (2009) The effect of phosphate content on the bioactivity of soda-lime-phosphosilicate glasses. *Journal of Materials Science: Materials in Medicine*, Vol.20, No.8, pp.1611-1618, ISSN 1573-4838.
- Padilla, S., Roman, J. & Vallet-Regi, M. (2002) Synthesis of porous hydroxyapatite by combination of gelcasting and foams burn out methods. *Journal of Materials Science: Materials in Medicine*, Vol.13, No.12, pp.1193-1197, ISSN 1573-4838.
- Pedone, A., Charpentier, T., Malavasi, G. & Menziani, M. C. (2010) New Insights into the Atomic Structure of 45S5 Bioglass by Means of Solid-State NMR Spectroscopy and Accurate First-Principles Simulations. *Chemistry of Materials*, Vol.22, No.19, pp.5644-5652, ISSN 1520-5002.
- Pedone, A., Malavasi, G., Cormack, A. N., Segre, U. & Menziani, M. C. (2008) Elastic and dynamical properties of alkali-silicate glasses from computer simulations techniques. *Theoretical Chemistry Accounts: Theory, Computation, and Modeling (Theoretica Chimica Acta)*, Vol.120, No.4-6, pp.557-564, ISSN 1432-2234.
- Pedone, A., Malavasi, G., Menziani, M. C., Segre, U. & Cormack, A. N. (2008) Role of Magnesium in soda-lime glasses: insight into structure, transport and mechanical properties through computer simulations. *The Journal of Physical Chemistry C*, Vol.112, No.29, pp.11034-11041, ISSN 1932-7447.
- Perdew, J. P., Burke, B. & Ernzerhof, M. (1996) Generalized Gradient Approximation Made Simple. *Physical Review Letters*, Vol.77, No.18, pp.3865-3868, ISSN 1079-7114.
- Peroos, S., Du, Z. M. & de Leeuw, N. H. (2006) A computer modelling study of the uptake, structure and distribution of carbonate defects in hydroxy-apatite. *Biomaterials*, Vol.27, No.9, pp.2150-2161, ISSN 0142-9612.
- Rabone, J. A. L. & de Leeuw, N. H. (2005) Interatomic Potential Models for Natural Apatite Crystals: Incorporating Strontium and the Lanthanides. *Journal of Computational Chemistry*, Vol.27, No.2, pp.253-266, ISSN 1096-987X.
- Rabone, J. A. L. & de Leeuw, N. H. (2007) Potential routes to carbon inclusion in apatite minerals: a DFT study. *Physics and Chemistry of Minerals*, Vol.34, No.7, pp.495-506, ISSN 1432-2021.
- Rimola, A., Corno, M., Zicovich-Wilson, C. M. & Ugliengo, P. (2008) *Ab Initio* Modeling of Protein/Biomaterial Interactions: Glycine Adsorption at Hydroxyapatite Surfaces. *Journal of the American Chemical Society*, Vol.130, No.48, pp.16181-16183, ISSN 0002-7863.
- Rimola, A., Corno, M., Zicovich-Wilson, C. M. & Ugliengo, P. (2009) *Ab initio* modeling of protein/biomaterial interactions: competitive adsorption between glycine and water onto hydroxyapatite surfaces. *Physical Chemistry Chemical Physics*, Vol.11, No.40, pp.9005 - 9007, ISSN 1463-9084.

- Rodriguez-Lorenzo, L. M., Vallet-Regi, M., Ferreira, J. M. F., Ginebra, M. P., Aparicio, C. & Planell, J. A. (2002) Hydroxyapatite ceramic bodies with tailored mechanical properties for different applications. *Journal of Biomedical Materials Research A*, Vol.60, 159-166, ISSN 1097-4636.
- Roveri, N. & Palazzo, B. (2006). Hydroxyapatite Nanocrystals as Bone Tissue Substitute. In *Tissue, Cell and Organ Engineering*, C.S.S.R. Kumar (Ed.), pp. 283-307, Wiley-VCH, ISBN 978-3-527-31389-1, Weinheim.
- Sakhno, Y., Bertinetti, L., Iafisco, M., Tampieri, A., Roveri, N. & Martra, G. (2010) Surface Hydration and Cationic Sites of Nanohydroxyapatites with Amorphous or Crystalline Surfaces: A Comparative Study. *The Journal of Physical Chemistry C*, Vol.114, No.39, pp.16640-16648, ISSN 1932-7447.
- Sato, K., Kogure, T., Iwai, H. & Tanaka, J. (2002) Atomic-Scale {101-0} Interfacial Structure in Hydroxyapatite Determined by High-Resolution Transmission Electron Microscopy. *Journal of the American Ceramic Society*, Vol.85, No.12, pp.3054-3058, ISSN 1551-2916.
- Suda, H., Yashima, M., Kakihana, M. & Yoshimura, M. (1995) Monoclinic <--> Hexagonal Phase Transition in Hydroxyapatite Studied by X-ray Powder Diffraction and Differential Scanning Calorimeter Techniques. *The Journal of Physical Chemistry*, Vol.99, No.17, pp.6752-6754, ISSN 0022-3654.
- Tadic, D., Beckmann, F., Schwarz, K. & Epple, M. (2004) A novel method to produce hydroxyapatite objects with interconnecting porosity that avoids sintering. *Biomaterials*, Vol.25, No.16, pp.3335-3340, ISSN 0142-9612.
- Tilocca, A. (2010) Models of structure, dynamics and reactivity of bioglasses: a review. *Journal of Materials Chemistry*, Vol.20, No.33, pp.6848-6858, ISSN 0959-9428.
- Tilocca, A. & Cormack, A. N. (2007) Structural effects of Phosphorus Inclusion in Bioactive Silicate Glasses. *The Journal of Physical Chemistry B*, Vol.111, No.51, pp.14256-14264, ISSN 1520-6106.
- Tilocca, A. & Cormack, A. N. (2009) Surface Signatures of Bioactivity: MD Simulations of 45S and 65S Silicate Glasses. *Langmuir*, Vol.26, No.1, pp.545-551, ISSN 0743-7463.
- Toulhat, N., Potocek, V., Neskovic, M., Fedoroff, M., Jeanjean, J. & Vincent, V. (1996) Perspectives for the study of the diffusion of radionuclides into minerals using the nuclear microprobe techniques. *Radiochimica Acta*, Vol.74, No.1, pp.257-262, ISSN 0033-8230.
- Ugliengo, P., Viterbo, D. & Chiari, G. (1993) MOLDRAW: Molecular Graphics on a Personal Computer. *Zeitschrift fur Kristallographie*, Vol.207, No.1, pp.9-23, ISSN 0044-2968.
- Wahl, D. A., Sachlos, E., Liu, C. & Czernuszka, J. T. (2007) Controlling the processing of collagen-hydroxyapatite scaffolds for bone tissue engineering. *Journal of Materials Science: Materials in Medicine*, Vol.18, 201-209, ISSN 1573-4838.
- Weiner, S. & Wagner, H. D. (1998) The material bone: structure-mechanical function relations. *Annual Review of Materials Science*, Vol.28, No.1, pp.271-298, ISSN 0084-6600.
- Wierzbicki, A. & Cheung, H. S. (2000) Molecular modeling of inhibition of hydroxyapatite by phosphocitrate. *Journal of Molecular Structure: THEOCHEM*, Vol.529, No.1-3, pp.73-82, ISSN 0166-1280.
- Young, R. A. & Brown, W. E. (1982). Structures of Biological Minerals. In *Biological Mineralization and Demineralization*, G.H. Nancollas (Ed.), pp. 101-141, Springer-Verlag, ISBN 978-0387115214, Berlin, Heidelberg, New York.



Biomaterials - Physics and Chemistry

Edited by Prof. Rosario Pignatello

ISBN 978-953-307-418-4

Hard cover, 490 pages

Publisher InTech

Published online 14, November, 2011

Published in print edition November, 2011

These contribution books collect reviews and original articles from eminent experts working in the interdisciplinary arena of biomaterial development and use. From their direct and recent experience, the readers can achieve a wide vision on the new and ongoing potentialities of different synthetic and engineered biomaterials. Contributions were selected not based on a direct market or clinical interest, but based on results coming from very fundamental studies. This too will allow to gain a more general view of what and how the various biomaterials can do and work for, along with the methodologies necessary to design, develop and characterize them, without the restrictions necessarily imposed by industrial or profit concerns. The chapters have been arranged to give readers an organized view of this research area. In particular, this book contains 25 chapters related to recent researches on new and known materials, with a particular attention to their physical, mechanical and chemical characterization, along with biocompatibility and histopathological studies. Readers will be guided inside the range of disciplines and design methodologies used to develop biomaterials possessing the physical and biological properties needed for specific medical and clinical applications.

How to reference

In order to correctly reference this scholarly work, feel free to copy and paste the following:

Marta Corno, Fabio Chiatti, Alfonso Pedone and Piero Ugliengo (2011). In Silico Study of Hydroxyapatite and Bioglass®: How Computational Science Sheds Light on Biomaterials, *Biomaterials - Physics and Chemistry*, Prof. Rosario Pignatello (Ed.), ISBN: 978-953-307-418-4, InTech, Available from:
<http://www.intechopen.com/books/biomaterials-physics-and-chemistry/in-silico-study-of-hydroxyapatite-and-bioglass-how-computational-science-sheds-light-on-biomaterials>

INTECH
open science | open minds

InTech Europe

University Campus STeP Ri
Slavka Krautzeka 83/A
51000 Rijeka, Croatia
Phone: +385 (51) 770 447
Fax: +385 (51) 686 166
www.intechopen.com

InTech China

Unit 405, Office Block, Hotel Equatorial Shanghai
No.65, Yan An Road (West), Shanghai, 200040, China
中国上海市延安西路65号上海国际贵都大饭店办公楼405单元
Phone: +86-21-62489820
Fax: +86-21-62489821

© 2011 The Author(s). Licensee IntechOpen. This is an open access article distributed under the terms of the [Creative Commons Attribution 3.0 License](#), which permits unrestricted use, distribution, and reproduction in any medium, provided the original work is properly cited.

IntechOpen

IntechOpen